

Solution grown nanocrystalline ZnO thin films for UV emission and LPG sensing

S. B. Patil · A. K. Singh

Received: 31 December 2009 / Accepted: 26 April 2010 / Published online: 25 May 2010
© Springer Science+Business Media, LLC 2010

Abstract Nanocrystalline ZnO thin films were successfully deposited by a simple and inexpensive solution growth technique. Photoluminescence (PL) and liquefied petroleum gas (LPG) sensing properties were investigated. Films were found to be uniform, pinhole free, and well adherent. As deposited and heat treated (at 673 K for 2 h) films were characterized by XRD, SEM, and EDAX. The dc electrical resistivity and LPG sensing property were measured. The change in morphology, from spherical particle to rod-like, was observed after air annealing. XRD results revealed that the obtained films were nanocrystalline and had a hexagonal wurtzite structure. The absorption edge was found to be at around 366 nm for the as-deposited film and 374 nm for the annealed film. The band gaps were found to be 3.29 and 2.9 eV for the as-deposited and annealed films, respectively. PL spectra of ZnO thin films showed strong peak at 384 nm, which corresponds to near band edge emission (UV emission) and a relatively weak peak at 471 nm. Further, the annealed film was used for detection of LPG in air. Maximum response was observed at 673 K. The maximum sensitivity of sensor was found to be 4.5 for 0.6 vol.% LPG. Sensing response got saturated after 0.6 vol.% of gas concentration. A possible mechanism of LPG sensing has been explained.

Introduction

The recent concerns on environmental pollution and increased awareness over the need to monitor potentially hazardous gases have stimulated considerable research and

development in the field of gas sensors. Thin films are suitable for such sensors as the gas sensing properties are related to the material surface and the gases are adsorbed and react with the surface of the film [1]. Thin film-based gas sensors have better sensitivity [2] as compared to conventional sintered bulk gas sensors. Furthermore, development of gas sensors to monitor combustible gases is important due to the concern for safety requirements in homes and in industries, particularly for detection of liquefied petroleum gas (LPG), which is one of the most extensively used but potentially hazardous gases, leading to accidents on leakage. Thus, the detection of LPG in domestic appliances must be reliable with no false or missing alarms. Semiconductors such as SnO₂ and ZnO [3, 4] have been widely studied for gas sensing applications. ZnO is preferred to SnO₂ as the latter is toxic in nature. The gas detection mechanism in ZnO nanostructures is based on alteration of their electrical properties due to the adsorption of oxidizing or reducing species. In addition, electrical properties of ZnO also depend on oxygen vacancies, mobility, concentration of charge carriers, and surface states. An effective lowering of operation temperature and enhanced gas sensing ability can be obtained by modifying the surface morphology.

Besides gas sensing, ZnO is widely used in solar cells [5], spintronics [6], transparent conductive oxides (TCO) [7], piezoelectricity [8], field emission displays [9], photocatalysis [10], and PL [11]. Being biodegradable and biocompatible it is suitable for medical and biological applications. ZnO has direct and wide-band gap ($E_g = 3.37$ eV at room temperature) and high exciton binding energy of 60 meV which makes the exciton state stable even at room temperature.

Thin films of ZnO have been obtained by several methods such as radio frequency magnetron sputtering [12], metal–organic chemical vapor deposition (MOCVD)

S. B. Patil · A. K. Singh (✉)
Defence Institute of Advanced Technology
(Deemed University), Girinagar, Pune, MS 411025, India
e-mail: draksingh@hotmail.com; aksingh@diat.ac.in

[13], spray pyrolysis [14], thermal evaporation [15], sol gel [16], and hydrothermal process [17]. All these techniques require sophisticated equipments, increasing the cost of the process. For these reasons, solution growth techniques [18, 19] are advantageous because they are simple, convenient, suitable for large area deposition, and, most important, inexpensive. The control parameters are concentration of precursor chemicals and complexing agent, pH of the solution, deposition temperature, and time. With these parameters we can control the morphology, thickness of the films, and particle size. In this technique the small degree of supersaturation of the solutions causes the heterogeneous nucleation of the metal oxide on the substrate. The solubility of solutes can change as a result of chemical reactions within the solutions. When the solution reaches supersaturation, the solid particles are formed through nucleation and crystal growth takes place.

The physical and sensing properties of nanocrystalline ZnO are directly related to its preparation method, particle size, microstructure including morphology, crystal size, orientation, aspect ratio and crystalline density and operating temperature. In the present work we report the synthesis of ZnO thin films by a simple and inexpensive method, i.e., solution growth technique. As-deposited films were annealed at 673 K for 2 h and were utilized for PL and LPG sensing.

Experimental

Deposition of ZnO thin films

0.5 M aqueous solution of zinc acetate dihydrate extra pure (MERCK) was used as precursor. Triethanolamine (TEA) was used as complexing agent, and liquid ammonia was used to increase the pH of the solution to 12. Deposition temperature was 343 K with deposition time of 1 h. All solutions were prepared in double distilled (DD) water.

Amorphous glass microslides (Blue Star) of dimension 26 mm × 76 mm × 2 mm were initially washed with labagent detergent. Further these cleaned microslides were boiled in dilute chromic acid for 30 min and then washed with DD water. Finally substrates were rinsed with acetone before use.

Characterization

The as-deposited films were annealed in air atmosphere at 673 K for 2 h. Weight difference method was used to calculate the thickness of the thin films. Density of bulk ZnO was taken to be 5.98 g/cm³. Crystallographic study was carried out using Bruker AXS, Germany (Model D8 Advanced) diffractometer in the scanning range of 20–80°

(2θ) using Cu K_α radiations with wavelength 1.5045 Å. JEOL ASM 6360A Scanning Electron Microscope (SEM) was used to study the morphology of films. Room temperature optical absorption spectra of samples were recorded in the wavelength range of 300–900 nm using Hitachi-3200 spectrophotometer. The electrical resistivity measurement was carried out using two probe method with lab equipment unit in the temperature range of 300–623 K using Data Aquisition System (Data taker DT-80). The room temperature photoluminescence properties of both the films were studied using Perkin Elmer LS55 Luminescence Spectrometer in spectral range of 300–800 nm with a wavelength of 325 nm as an excitation source. A laboratory set up comprising of electric heater plate, K type thermocouple, temperature controller, gas flow-meter, and gas chamber was used to investigate the LPG sensing properties of ZnO thin film. Electrical resistance of the annealed ZnO film in air atmosphere and in the presence of LPG was measured using two-probe dc measurement method. Silver paste was applied to ensure good ohmic contacts with the films and the area of the films was defined (0.52 cm²) in both dc-electrical resistivity measurement and LPG sensing of the films.

Results and discussion

The crystal quality of the samples was studied by recording the XRD patterns in the range of 20–80°. Figure 1 shows the diffraction pattern of both the as-deposited and annealed ZnO film. Both the samples are polycrystalline and have a hexagonal structure (JCPDS 080-0074). Diffraction pattern of the as-deposited film shows peaks along (100), (002), and (101). There are no peaks along (211) and (013) indicating that Zn(OH)₂ phase formation has not taken place or it might be present in small extent in amorphous phase accumulated along the grain boundaries of the crystallites. The formation of Zn(OH)₂ phase was expected as all precursor solutions used were aqueous. From the diffraction pattern, it is clearly seen that the number of counts has increased and peaks have become narrow indicating the grain growth after air annealing. Similar type of behavior has been reported by Studenikin et al. [20]. The orientation of the film after air annealing has become prominent along (101). As can be seen from the Fig. 1 the diffraction peak counts from the (101) planes are increased significantly in comparison to other planes.

Scherrer's formula was used to calculate crystallite sizes (*D*) and is given by,

$$D = \frac{k\lambda}{\beta \cos\theta} \quad (1)$$

where constant *k* is 0.9, wavelength λ of the X-ray is 1.5045 Å, β is the Full Width Half Maximum (FWHM) (in

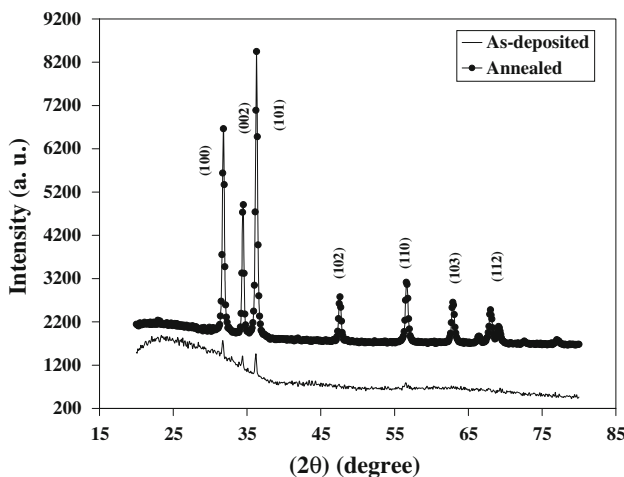


Fig. 1 XRD pattern of both the as-deposited and annealed thin films

radians) of the diffraction peak at 2θ degree. Average crystallite size was found to be 15 nm for the as-deposited film and 24 nm for the annealed film. To distinguish the effect of crystallite size-induced broadening and strain-induced broadening at FWHM of the XRD pattern, the Williamson–Hall plot has been performed and shown in Fig. 2. The strain can be obtained from the slope of the Williamson–Hall plot as;

$$\beta \cos \theta = 2\varepsilon \sin \theta + \frac{C\lambda}{D} \quad (2)$$

where β , θ , λ , and D have their usual meaning and C is correction factor taken as 1 and ε is strain. The strain of the as-deposited film was found to be 1.6×10^{-2} which is reduced to 2.9×10^{-3} after air annealing. The strain values are very small, as can be seen from the Williamson–Hall plot, and their effect on broadening is negligible. Similar results have been reported by Tan et al. [21]. Stoichiometry of ZnO thin films has been confirmed by EDAX spectra and is shown in Fig. 3.

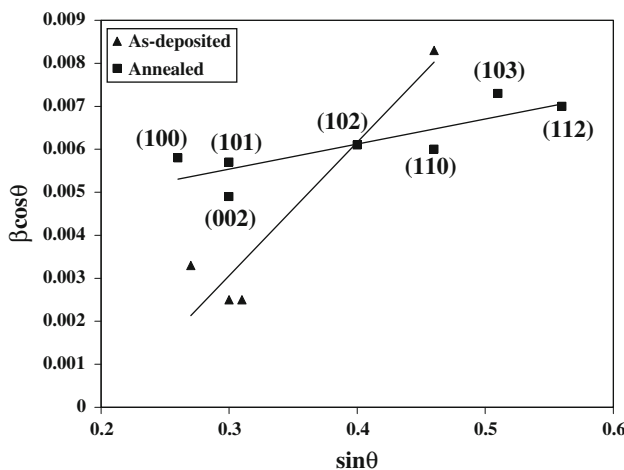


Fig. 2 Williamson–Hall plot for the as-deposited and annealed film

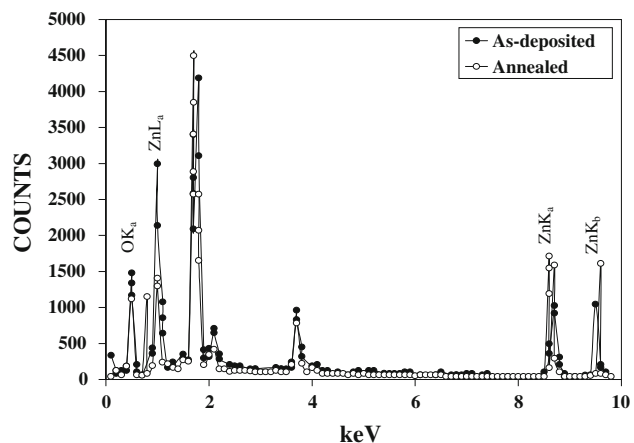


Fig. 3 EDAX of the as-deposited and annealed thin films

SEM micrographs of the as-deposited and annealed ZnO thin films are shown in Fig. 4a and b. The SEM micrograph of the as-deposited film (Fig. 4a) shows that the film is uniform, and the grains are spherical. The average grain size of the as-deposited film was in the range of about 80–200 nm. From these SEM micrographs high degree of agglomeration is also observed, which is peculiarity of metal oxide films deposited from aqueous solutions. Krotcenkov et al. [22] have reported similar behavior for the ZnO thin films grown by successive ionic layer deposition. The morphology of the annealed samples changed significantly from spherical to rod-like structures. The grain size increased significantly after annealing (Fig. 4b) which may be attributed to the merging of smaller grains into larger ones due to sufficient thermal energy. Similar results have been reported by Ghosh et al. [23] and Zhi et al. [24]. The grain sizes observed from the SEM micrographs are comparatively larger than the crystallite sizes calculated from Scherrer's formula for the as-deposited and annealed films [23]. This can be attributed to the presence of amorphous phase around the crystallites [23]. The XRD results strongly support the SEM results.

Optical absorption spectra of both the as-deposited and annealed ZnO thin films have been studied without taking into account the reflection and transmission losses. Tuac's relation of the absorption coefficient (α) with the photon energy (hv) has been used to determine the band gap energy of both the samples and is given by,

$$\alpha = \frac{\alpha_0(hv - E_g)^n}{hv} \quad (3)$$

where α is the absorption coefficient, α_0 is the constant, hv is the photon energy, and E_g is the band gap energy of the material. The value of n depends on the probability of transition; it takes values as 1/2, 3/2, 2, and 3 for direct allowed, direct forbidden, indirect allowed, and indirect forbidden, respectively. The variation of $(\alpha h v)^2$ versus $h v$

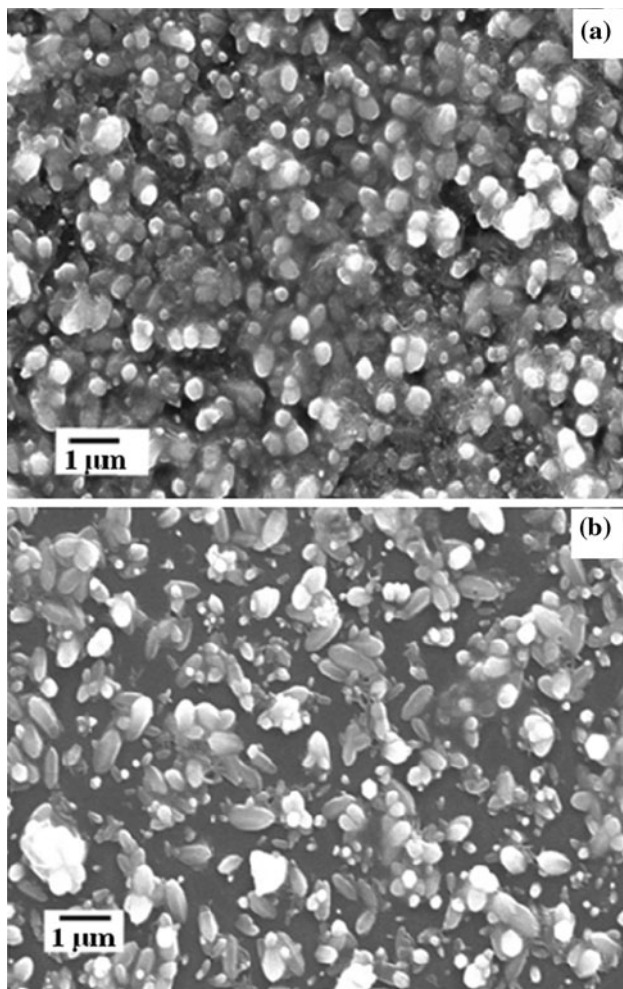


Fig. 4 SEM micrograph of **a** as-deposited and **b** annealed thin films

for both the samples is depicted in Fig. 5. Both the as-deposited and annealed zinc oxide thin films show low absorbance in the visible region, which is one of the characteristics of ZnO. The variation of $(\alpha h\nu)^2$ versus $h\nu$ is linear at the absorption edge which confirms that ZnO is semiconductor with direct band gap. Extrapolating the straight-line portion from higher absorption region of the plot $(\alpha h\nu)^2$ versus $h\nu$ to photon energy axis for zero absorption coefficient value gives the E_g . E_g of as-deposited and annealed thin film was found to be 3.29 and 2.97 eV, respectively. The relative high band gap energy in case of the as-deposited film may be due to the presence of zinc hydroxide in amorphous phase [23]. The decrease in band gap energy after air annealing can be attributed to increase in grain size and/or removal of zinc hydroxide and/or removal of defects [25]. The decrease in band gap shows that the annealing has resulted in 0.39 eV red shift in the optical absorption [21].

The dc electrical resistivity measurement has been carried out using two probe method in the temperature range

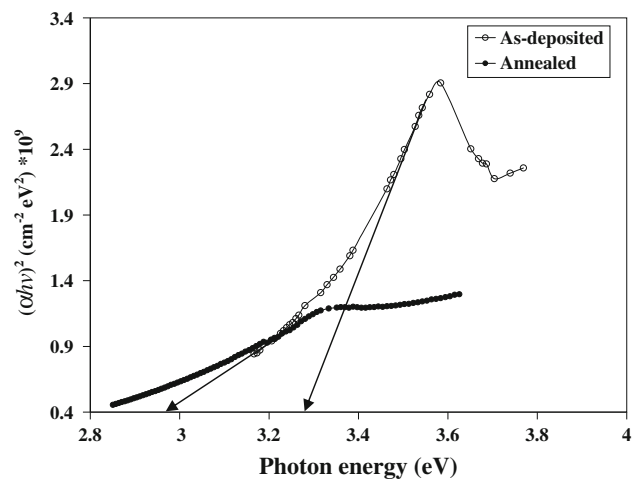


Fig. 5 Plot of $(\alpha h\nu)^2$ vs. photon energy ($h\nu$) for the (open circle) as-deposited, and (filled circle) annealed thin film

of 300–623 K. The temperature dependence of the electrical resistivity can be described by the well-known exponential law,

$$\rho = \rho_0 \exp\left(\frac{E_a}{k_B T}\right) \quad (4)$$

where ρ_0 is the constant depending on the sample characteristics (thickness, structure, etc.), k_B is the Boltzmann constant, T is the absolute temperature, and E_a is the activation energy for electrical conduction. Activation energy is the amount of thermal energy required to release an electron from trap level to the conduction band (CB). These trap levels are the levels located few meV below the CB in the forbidden region and are nothing but the crystal defects [26]. Ohmic behavior of the contacts are confirmed by checking the current (I)–voltage (V) characteristic across the contacts which show a linear dependence of current on applied voltage. A plot of $\log \rho$ versus $10^3/T$ for the annealed ZnO thin film shown in Fig. 6 indicates the semiconducting nature of the ZnO thin film. The room temperature resistivity was found to be $10 \text{ M}\Omega \text{ cm}$. This high resistivity may be due to nanocrystalline nature of the sample. Decrease in the resistivity was found after annealing of the thin films which is due to grain growth in turn increase in crystallite size, as evident from the XRD results. The activation energy (E_a) was found to be 0.9 eV.

Photoluminescence technique is suitable to determine the crystalline quality and presence of impurities in the materials, as well as, exciton fine structure. The room temperature PL spectra for the as-deposited and annealed thin film are represented in Fig. 7. A strong peak around 384 nm for the as-deposited film is the near band edge emission (UV emission) due to the free-exciton recombination. After air annealing, near band edge emission was shifted to higher wavelength, i.e., 390 nm. This red shift is

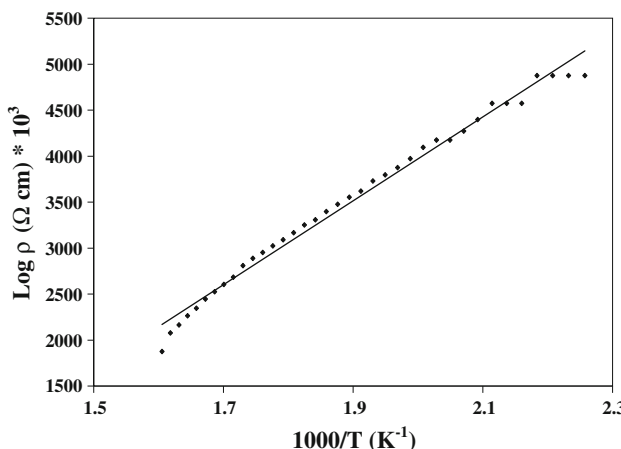


Fig. 6 Plot of $\log \rho$ versus $10^3/T$ for the annealed thin film

similar to the red shift in the optical absorption spectrum which can be attributed to change in the shape and size of the nanocrystals [27]. The presence of the relatively weak peaks at 410 and 423 nm can be attributed to defects such as zinc vacancies and anti-sites zinc–oxygen. Similar peaks around 390 and 410 were reported by Singh et al. [28] for the ZnO nanoparticles. The blue emission at 470 nm is attributed to intrinsic defects such as oxygen and zinc interstitials. The peak around 520 nm is the green emission and usually due to surface defects, oxygen vacancies which can trap the electrons from the valence band and act as luminescent center. Generally, a green-yellow emission is observed in PL spectra, due to recombination of photo generated holes with singly ionized charge state of specific defect. Similar type of PL emission has been reported by Hwangbo et al. [29] for sol-gel-derived ZnO thin films.

The change in resistance of a semiconductor oxide, such as ZnO, in the presence of target gas takes place according

to two reactions [30]. In the first reaction atmospheric (atm) oxygen, O_2 , molecules are adsorbed on the surface by taking electron from the conduction band (CB) and thus chemisorbed on the surface as O_{ads}^- , this leads to increase in resistance of the sensor material. The chemical reaction can be explained by equation below



In second reaction, the reducing gases (R) present in the target gas injected into the reaction chamber reacts with the chemisorbed oxygen, O_{ads}^- , thereby releasing an electron back to the conduction band and decreasing the resistance of the sensor material given by Eq. 5. LPG consists of CH_4 , C_3H_8 , and C_4H_{10} molecules and in these molecules the reducing hydrogen species are bound to carbon atoms. These molecules react with chemisorbed oxygen, O_{ads}^- , and release an electron to CB. The overall reaction of LPG molecules with adsorbed oxygen can be explained in a similar way by equation below

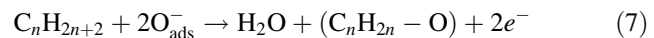
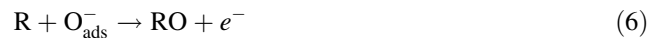


Figure 8 shows the LPG sensing response of the annealed ZnO film with temperature at different gas concentrations. The sensitivity (S) is defined as follows

$$S = \frac{R_a}{R_g} \quad (8)$$

where, R_g is the electrical resistance in presence of LPG in air atmosphere and R_a is the electrical resistance in air atmosphere only. It can be seen from figure that the sensing response is increased with temperature up to 673 K and decreased thereafter for all gas concentrations. The low sensing response at the temperatures below 673 K for all gas concentrations can be attributed to insufficient thermal

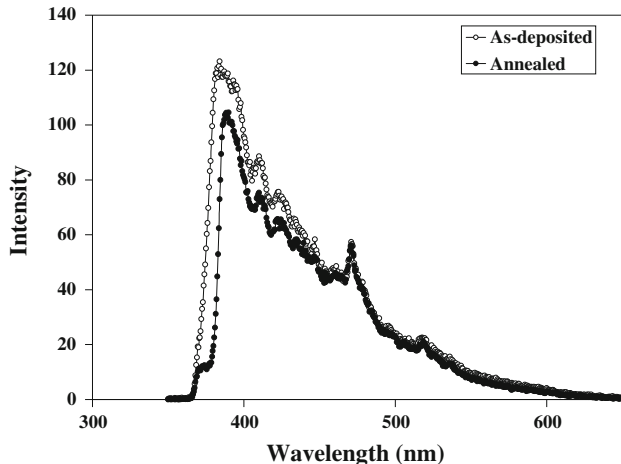


Fig. 7 Room temperature PL spectra of both the as-deposited and annealed thin films. A wavelength of 325 nm is used as an excitation source

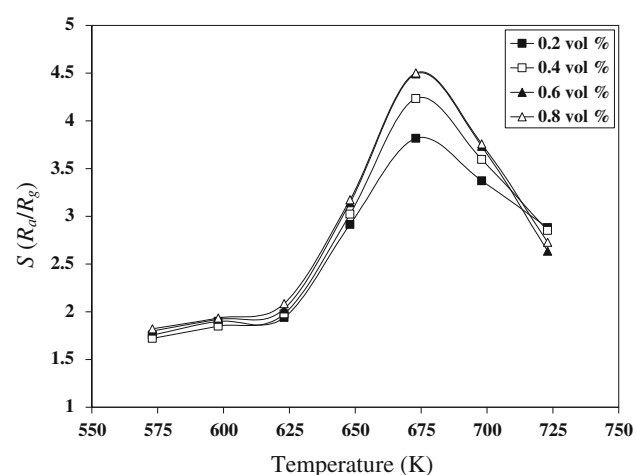


Fig. 8 Sensing response of the annealed film with temperature at different gas concentrations

energies for LPG molecules to react with the surface adsorbed oxygen molecules as per Eq. 7. Whereas the reduction in the sensing response after 673 K for all gas concentrations may be due to higher thermal energies which desorb the LPG molecules from the ZnO film surface. The adsorbed oxygen on the ZnO film drags the electrons from the conduction band and forms a potential barrier to charge transport. The thermal energy at lower temperatures is not sufficient to overcome the potential barrier, while at higher temperatures the higher thermal energy restricts the diffusion of LPG molecules to the film surface. At some intermediate temperature the thermal energy and diffusion of the gas molecules becomes optimal and the sensor response reaches its maximum value. In this case sensor response reached its maxima at 673 K. This temperature is called optimal temperature at which adsorption of the LPG molecules is maximum and thermal energy is enough to complete the chemical reaction as per Eq. 7, which led to maximum sensitivity. Above the optimal temperature the diffusion of LPG molecules to the film is restricted which led to decrease in the sensitivity. The increase and decrease in the sensitivity observed in the figure indicates the adsorption and desorption phenomenon of the gases.

Similar behavior has been reported by Shinde et al. [31]. The obtained results are better than the earlier report by Sun et al. [32] for the ZnO nanorods synthesized by solid-state reaction for LPG sensing. The sensor response with gas concentration at 673 K is depicted in Fig. 9. It is clear from this figure that the sensitivity of the sensor increased with increasing gas concentration up to 0.6 vol.% and saturated thereafter. The sensitivity for 0.2 vol.% of LPG was found to be 3.8, 4.3 for 0.4 vol.% and was maximum 4.5 for 0.6 vol.% and saturated thereafter. The saturation in the sensing response after 0.6 vol.% of gas concentration can be attributed to limited reaction sites on the film surface.

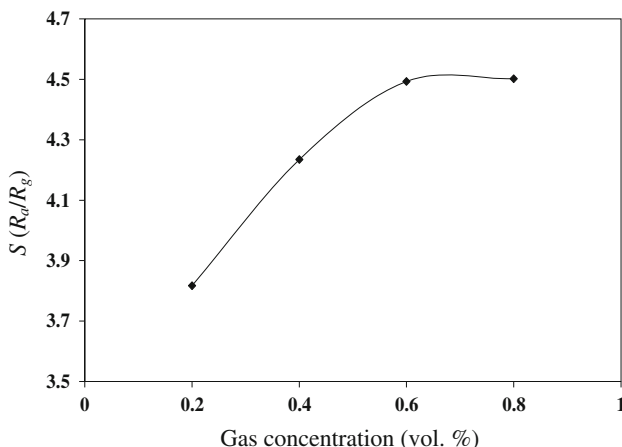


Fig. 9 Sensing response of the annealed film with gas concentration at 673 K

Conclusions

Solution growth technique has provided uniform, pinhole free and well adherent nanocrystalline ZnO thin films. XRD results show that the obtained films exhibit hexagonal wurtzite phase with average crystallite size 15 nm for as-deposited film and 24 nm for annealed film. Orientation of ZnO nano-crystallites was prominent along (101) after air annealing. SEM results show that the morphology of the annealed samples changed significantly from spherical to rod-like structures. PL spectra of ZnO thin films show strong UV emission and relatively weak green emission indicating good quality of films with little surface defects. Slight red shift in the UV emission was observed after annealing. The ratio of the intensity of the UV emission to green emission is about 6. Thus, these samples can be used as low cost UV emitters. The annealed film was successfully used for LPG detection. The operating temperature was found to be 673 K. Maximum sensor sensitivity was found to be 4.5 for 0.6 vol.% of gas concentration and saturated thereafter.

Acknowledgement Authors are thankful to Vice Chancellor, Defence Institute of Advanced Technology, Girinagar, Pune-411025 (India) for granting permission to publish this work. Authors are also thankful to Department of Physics, University of Pune, Pune (India), for XRD and photoluminescence measurement of thin films and valuable discussions.

References

- Liu XQ, Tao SW, Shen YS (1997) *Sens Actu B* 40:161
- Chai CC, Peng J, Yan BP (1995) *J Electron Mater* 24:799
- Choi YJ, Hwang IS, Park JG, Choi KJ, Park JH, Lee JH (2008) *Nanotechnology* 19:095508
- Ferro R, Rodríguez JA, Bertrand P (2008) *Thin Solid Films* 516:2225
- Suh DI, Lee SY, Kim TH, Chum JM, Suh EK, Yang OB, Lee SK (2007) *Chem Phys Lett* 442:348
- Sharma P, Gupta A, Owens FJ, Inoue A, Rao KV (2004) *J Magn Magn Mater* 282:115
- Guillen C, Herrero J (2008) *J Vacuum* 82:668
- Zhao M, Wang Z, Mao SX (2004) *Nano Lett* 4:587
- Lee CJ, Lee TJ, Lyu SC, Zhang Y, Ruh H, Lee HJ (2002) *Appl Phys Lett* 81:3648
- Daneshvar N, Salari D, Khataee AR (2004) *J Photochem Photobiol A: Chem* 162:317
- Peng X, Xu J, Zang H, Wang B, Wang Z (2008) *J Lumin* 128:297
- Winfried H, Horsthuis G (1986) *Thin Solid Films* 137:185
- Kashiwaba Y, Haga K, Watanabe H, Zhang BP, Segawa Y, Wakatsuki K (2002) *Phys Status Solidi (b)* 229:921
- Paraguay F, Estrada W, Acosta LDR, Andrade NE, Yoshida MM (1999) *Thin Solid Films* 350:192
- Zhao J, Hu L, Wang Z, Zhao Y, Liang X, Wang M (2004) *Appl Surf Sci* 229:311
- Berber M, Bulto V, Kli R, Hahn H (2005) *Scrip Mater* 53:547
- Guo M, Diao P, Wang X, Cai S (2005) *J Sol Stat Chem* 178:3210
- Patra MK, Manzoor K, Manoth M, Vadera SR, Kumar N (2008) *J Lumin* 128:267

19. Zhang R, Pan J, Briggs EP, Thrash M, Kerr LL (2008) Sol Energy Mater Sol Cells 92:425
20. Studenikin SA, Golego N, Cociverab M (1998) J Appl Phys 84/4:2287
21. Tan ST, Chen BJ, Sun XW, Ean WJ, Kwok HS, Zhang XH, Chssua SJ (2005) J Appl Phys 98:013505
22. Korotcenkov G, Tolstoy V, Schwank J (2006) Meas Sci Technol 17:1861
23. Ghosh A, Deshpande NG, Gudage YG, Joshi RA, Sagade AA, Phase DM, Sharma R (2009) J Alloy Comp 469:56
24. Zhi ZZ, Liu YC, Li BS, Zhang XT, Lu YM, Shen DZ, Fan XW (2003) J Phys D Appl Phys 36:719
25. Kanade KG, Kale BB, Aiyer RC, Das BK (2006) Mater Res Bull 41:590
26. Shinde VR, Lokhande CD, Mane RS, Han SH (2005) Appl Surf Sci 245:407
27. Djurišić AB, Leung YH (2006) Small 8–9:944
28. Singh AK, Viswanath V, Janu VC (2009) J Lumin 129:874
29. Hwangbo S, Lee YJ, Hwang KS (2008) Ceram Inter 34:1237
30. Garje AD, Aiyer RC (2006) Int J Appl Ceram Technol 3:477
31. Shinde VR, Gujar TP, Lokhande CD (2007) Sens Actu B 120:551
32. Sun ZP, Liu L, Zhang L, Jia DZ (2006) Nanotechnology 17:2266